

## SWORD M-SCH-B2735 - P-RICH IRON - IRON AGE - SWITZERLAND

<b>Artefact name</b>	Sword M-Sch-B2735
<b>Authors</b>	Marianne. Senn (EMPA, Dübendorf, Zurich, Switzerland) & Christian. Degriigny (HE-Arc CR, Neuchâtel, Neuchâtel, Switzerland)
<b>Url</b>	/artefacts/531/

### ∨ The object



Credit HE-Arc CR.

Fig. 1: Sword (after Senn Bischofberger 2005, 241),

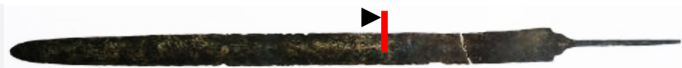
### ∨ Description and visual observation

<b>Description of the artefact</b>	Sword of the middle la Tène type, broken into two parts (Fig. 1). Under a hand lens the surface shows parallel grinding traces from mechanical cleaning.
<b>Type of artefact</b>	Weapon
<b>Origin</b>	Marin-Epagnier, La Tène, Saint-Blaise, Neuchâtel, Switzerland
<b>Recovering date</b>	Water finds, end 19th/beginning 20th cent. AD
<b>Chronology category</b>	Iron Age
<b>chronology tpq</b>	<input type="text" value="250"/> B.C. ∨
<b>chronology taq</b>	<input type="text" value="140"/> B.C. ∨
<b>Chronology comment</b>	La Tène C
<b>Burial conditions / environment</b>	Soil
<b>Artefact location</b>	Museum Schwab, Biel/Bienne, Bern
<b>Owner</b>	Museum Schwab, Biel/Bienne, Bern
<b>Inv. number</b>	M-Sch-B2735
<b>Recorded conservation data</b>	Conserved (not recorded, but mechanical cleaning visible)

### Complementary information

Nothing to report.

### ∨ Study area(s)



Credit HE-Arc CR.

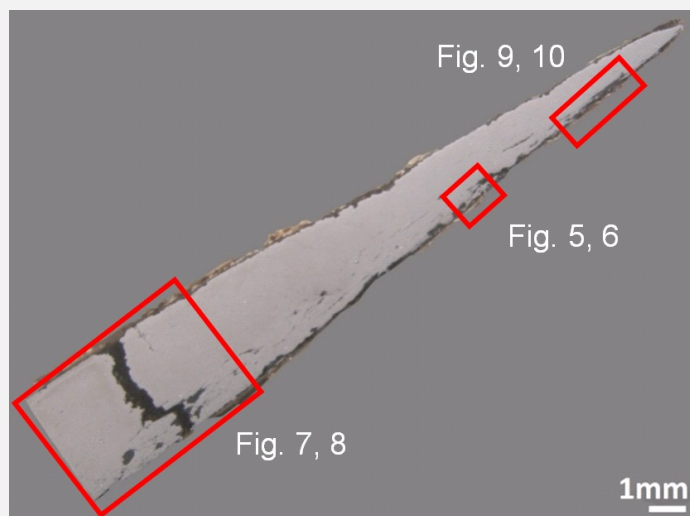
Fig. 2: Location of sampling area,

✧ Binocular observation and representation of the corrosion structure

Stratigraphic representation: none.

✧ MiCorr stratigraphy(ies) – Bi

✧ Sample(s)



Credit HE-Arc CR.

Fig. 3: Micrograph of the cross-section of the sample taken from the sword showing the location of Figs. 5 to 10,

<b>Description of sample</b>	The sample includes half of the sword blade (Figs. 2 and 3). The corrosion layer is thin (Fig. 3).
<b>Alloy</b>	P-rich iron
<b>Technology</b>	Forged, annealed and cold worked
<b>Lab number of sample</b>	M-SCH-B2735
<b>Sample location</b>	Empa (Marianne Senn)
<b>Responsible institution</b>	Schweizerisches Landesmuseum, Zürich, Zurich
<b>Date and aim of sampling</b>	1969, metallography

**Complementary information**

Nothing to report.

✧ Analyses and results

**Analyses performed:**

Metallography (nital etched), Vickers hardness testing, LA-ICP-MS, SEM/EDS.

∨ Non invasive analysis

∨ Metal

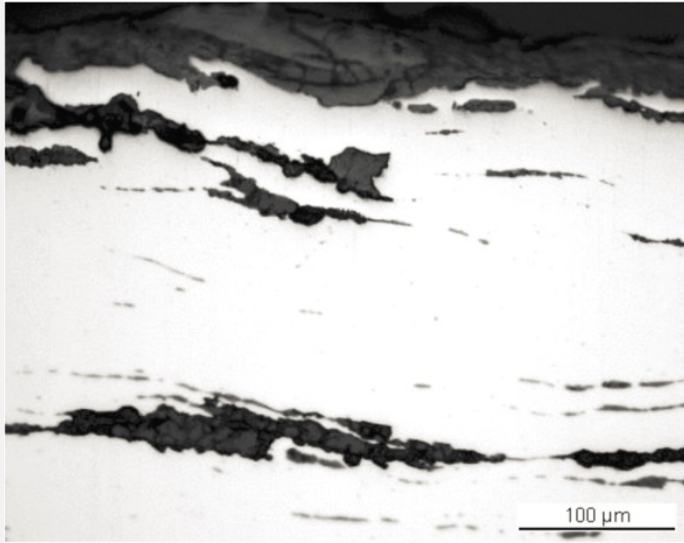
The remaining metal is a P-rich (0.2 mass%) iron (Table 1) with long parallel slag inclusions (Fig. 5) concentrated on one side of the blade. The slag inclusions are composed of wüstite/FeO dendrites and fayalite/Fe<sub>2</sub>SiO<sub>4</sub> in a glassy matrix (Fig. 6 and Table 2). Their chemical composition is typical for iron produced by the bloomery process (dominated by iron oxides and silica). It is difficult to identify the ore type from the slag composition. Interestingly in one case the slag composition is very specific (alumina and P-rich material). After etching, the metal shows a ferritic structure (Fig. 7). The grain size is variable (between ASTM grain sizes of 4 to 7) and some grains include Neumann bands (Fig. 8). A large crack has developed through the metal section (Figs. 3 and 7). The average hardness of the metal (HV1 185) is quite high for a wrought iron. The level of hardness and Neumann bands are typical for a P-rich iron. Neumann bands are said to develop by cold working and shock deformation. According to Swiss and McDonnell 2003 they form when little cold work is carried out. Distortion (grain deformation) after cold working starts to be apparent in iron after a reduction in thickness of between 30-40%. Since no grain deformation is visible, the present reduction is probably a little less than this range.

Elements	V	Cr	Mn	P	Co	Ni	Cu	As	Ag
Median mg/kg	<	5	10	2200	140	270	500	260	<
Detection limit mg/kg	1	4	1	50	1	1	1	2	0.1
RSD %	-	56	48	10	14	16	37	15	-

Table 1: Chemical composition of the metal. Method of analysis: LA-ICP-MS, Lab Analytical Chemistry, Empa (for details see Devos et al. 2000).

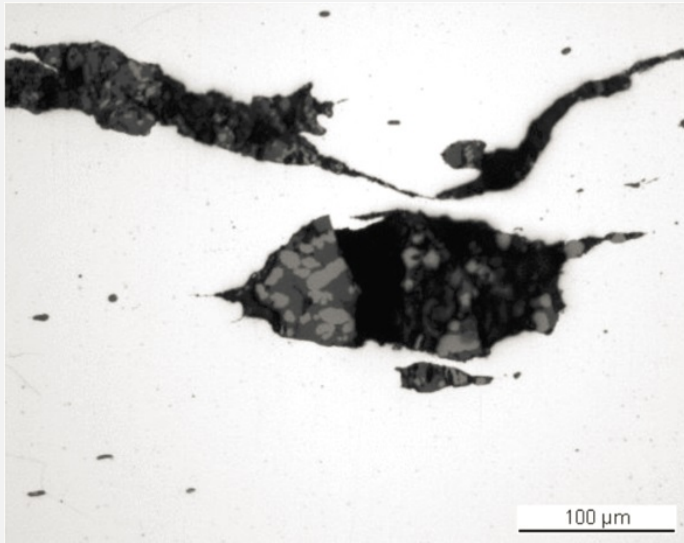
Structure	MgO	Al <sub>2</sub> O <sub>3</sub>	SiO <sub>2</sub>	P <sub>2</sub> O <sub>5</sub>	K <sub>2</sub> O	CaO	TiO <sub>2</sub>	MnO	FeO	Total	SiO <sub>2</sub> /Al <sub>2</sub> O <sub>3</sub>
Wüstite in glass	0.7	2.1	15	2.7	<	0.6	<	<	87	109	7.2
Wüstite and fayalite in glass	<	4.8	24	0.7	1	1.4	<	<	70	103	5.0
Wüstite and fayalite in glass	0.6	2.7	23	1.8	<	0.8	<	<	69	98	8.4
Fayalite in glass	<	5.6	26	2.8	0.8	1.4	<	<	72	110	4.8
Fayalite phase	0.8	1.0	31	1.2	0.7	1.1	<	0.8	69	106	33
Fayalite in glass	<	8.8	24	3.2	1.0	1.4	0.6	<	66	106	2.8

Table 2: Chemical composition of the slag inclusions (mass%) at the tip (pearlite) and the body (ferrite) of the knife. Method of analysis: SEM/EDS, Laboratory of Analytical Chemistry, Empa.



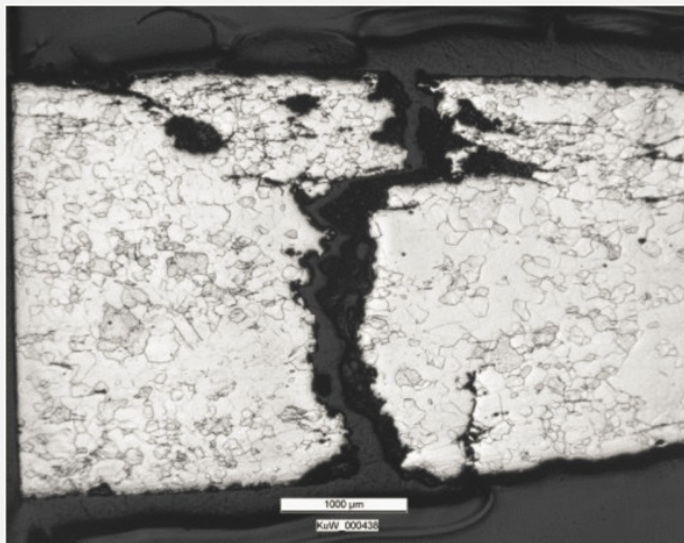
Credit HE-Arc CR.

Fig. 5: Micrograph of the metal sample from Fig. 3 (detail, rotated by 225°), unetched, bright field. In white the metal containing elongated slag inclusions (in grey); in black porosity,



Credit HE-Arc CR.

Fig. 6: Micrograph of the metal sample from Fig. 3 (detail), unetched, bright field. Detail with slag inclusions showing a structure with wüstite dendrite (light-grey) and fayalite (dark-grey),



Credit HE-Arc CR.

Fig. 7: Micrograph of the metal sample from Fig. 3 (reversed picture, rotated by 225°, detail), etched, bright field. Metal with a large pre-existing crack and ferritic, recrystallized structure. Grains have different sizes,

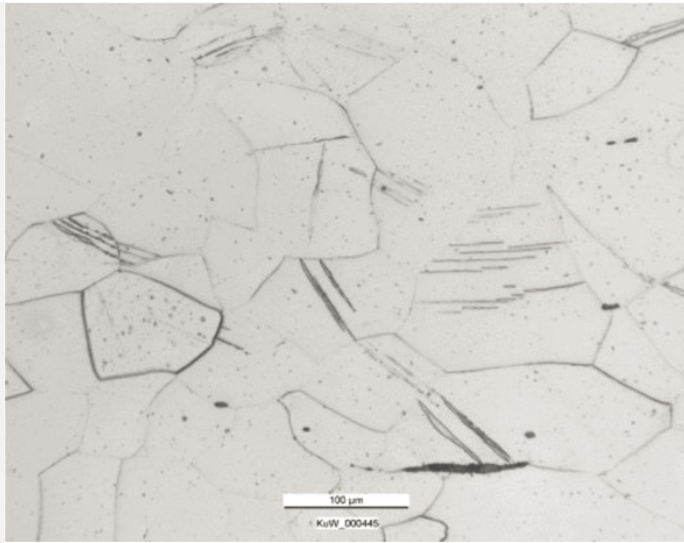


Fig. 8: Micrograph of the metal sample (detail of Fig. 7), etched, bright field. Ferrite grains including Neumann bands formed after cold working in a P-rich iron,

Credit HE-Arc CR.

<b>Microstructure</b>	Recrystallized grains, Newman bands, ghost structure
<b>First metal element</b>	Fe
<b>Other metal elements</b>	P

#### Complementary information

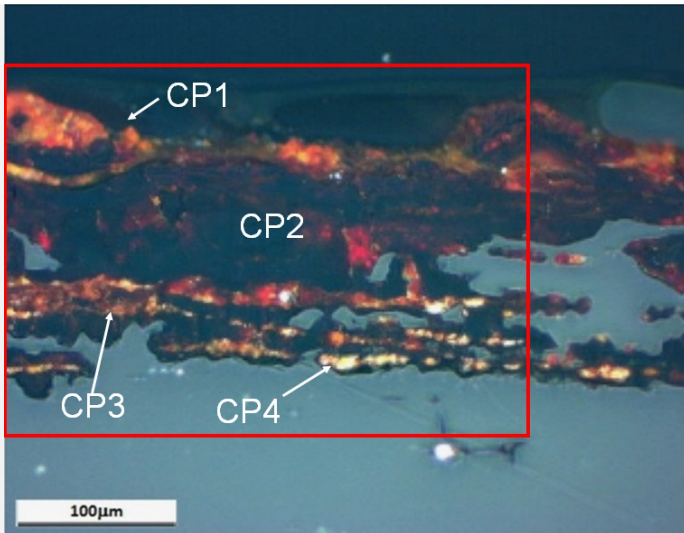
Nothing to report.

#### Corrosion layers

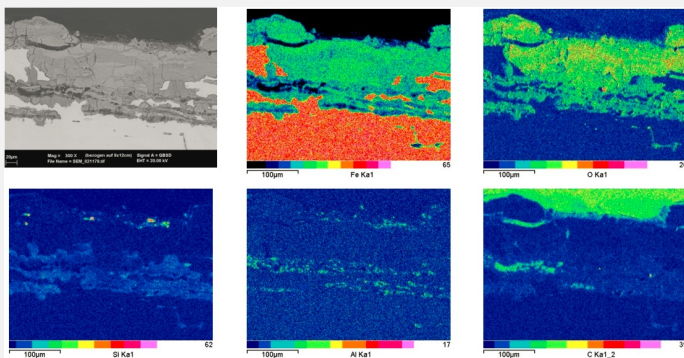
The remaining metal, including the large crack, is covered by a thin, fissured corrosion crust (Figs. 3, 5, 7 and 9). The corrosion crust is thicker on the side containing the long slag inclusions (Fig. 3). In bright field and in the BSE-mode of the SEM image only light and dark-grey areas can be distinguished (Figs. 5 and 10). Under polarised light the corrosion products appear yellow-orange near the metal surface and then become successively dark-red and black. The outer layer (CP1) is orange-yellow, as is the inner one (CP4, Fig. 9). There is a correlation between the level of grey in SEM/BSE-mode, the colours under polarised light, and the chemical composition of the corrosion layer (Table 3, Figs. 9 and 10). The lighter the grey of the SEM/BSE-mode, or the colours (light-brown and red) under polarised light, the richer the area is in Fe and the more depleted it is in O. Surprisingly the inner corrosion layers (CP3 and CP4) are contaminated with Si, Al and O.

Elements	O	Si	Fe	Total
Light or dark-red corrosion products (CP3)	25	1.6	67	94
Light or dark-red corrosion products (CP3)	32	<	74	108
Dark or dark-red corrosion products (CP2)	41	<	67	109

Table 3: Chemical composition (mass %) of the corrosion layer (from Fig. 9). Method of analysis: SEM/EDS, Laboratory of Analytical Chemistry, Empa.



Credit HE-Arc CR.



Credit HE-Arc CR.

Fig. 9: Micrograph showing the metal - corrosion crust interface from Fig. 3 (inverted picture, rotated by 135°, detail) and corresponding to the stratigraphy of Fig. 4, unetched, polarised light. The metal appears in blue and the corrosion changes from yellow-orange (CP4) to dark-red (CP3), black (CP2) and orange (CP1). The area selected for elemental chemical distribution (Fig. 10) is marked by a red rectangle,

Fig. 10: SEM image, BSE-mode, and elemental chemical distribution of the selected area from Fig. 9. Method of examination: SEM/EDS, Laboratory of Analytical Chemistry, Empa.,

**Corrosion form** Uniform - transgranular

**Corrosion type** ?

#### Complementary information

Nothing to report.

#### ∨ MiCorr stratigraphy(ies) – CS

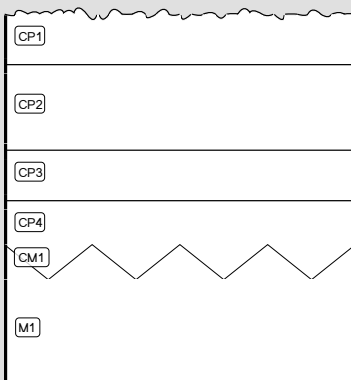


Fig. 4: Stratigraphic representation of the sample taken from the sword in cross-section using the MiCorr application. The characteristics of the strata are only accessible by clicking on the drawing that redirects you to the search tool by stratigraphy representation. This representation can be compared to Fig. 9, Credit HE-Arc CR.

#### ∨ Synthesis of the binocular / cross-section examination of the corrosion structure

Corrected stratigraphic representation: none.

## ∨ Conclusion

The sword blade is made of a hard, P-rich iron. It displays poor workmanship compared to other Celtic swords. The metal was first hot worked followed by a final cold working. The corrosion layer, typical of terrestrial context, has been partially removed by the conservation treatment. The possible use of air abrasive cleaning with glass beads and aluminium oxide, or the use of abrading tools, could explain the enrichment in Si and Al of the surface.

## ∨ References

### *References on object and sample*

#### **References object**

1. Senn Bischofberger, M. (2005) Das Schmiedehandwerk im nordalpinen Raum von der Eisenzeit bis ins frühe Mittelalter. Internationale Archäologie, Naturwissenschaft und Technologie Bd. 5, (Rahden/Westf.), 30.

#### **References sample**

2. Senn Bischofberger, M. (2005) Das Schmiedehandwerk im nordalpinen Raum von der Eisenzeit bis ins frühe Mittelalter. Internationale Archäologie, Naturwissenschaft und Technologie Bd. 5, (Rahden/Westf.), 240-242.

### *References on analytic methods and interpretation*

3. Swiss, A. J. and McDonnell, J.G. (2003) Evidence and interpretation of cold working in ferritic iron. International Conference, Archaeometallurgy in Europe 2003, Proceedings, vol. 1, Milan, 209-217.

4. ASTM E112-13: Standard Test Methods for Determining Average Grain Size.